

A quantum wire approach to weighted combinatorial graph optimisation problems

Johannes Kombe,^{1,*} Gerard Pelegrí,^{1,*} Andrew J. Daley,¹ and Jonathan D. Pritchard¹

¹*Department of Physics, SUPA and University of Strathclyde, Glasgow G4 0NG, United Kingdom*

Neutral-atom arrays have recently attracted attention as a versatile platform to implement coherent quantum annealing as an approach to hard problems, including combinatorial optimisation. Here we present an efficient scheme based on chains of Rydberg-blockaded atoms, which we call quantum wires, to embed certain weighted optimisation problems into a layout compatible with the neutral atom architecture. For graphs with quasi-unit-disk connectivity, in which only a few non-native long-range interactions are present, our approach requires a significantly lower overhead in the number of ancilla qubits than previous proposals, facilitating the implementation in currently available hardware. We perform simulations of realistic annealing ramps to find the solution of combinatorial optimisation problems within our scheme, demonstrating high success probability for problems of moderate size. Furthermore, we provide numerical evidence of a favourable scaling of the minimum gap along the annealing path with increasing wire length and of the robustness of the encoding to experimental imperfections. Our work expands the existing toolkit to explore the potential use of neutral atom arrays to solve large scale optimisation problems.

I. INTRODUCTION

Combinatorial optimisation problems are of great relevance across a wide range of scientific fields and industry sectors [1]. In many cases, these problems have been shown to be NP-hard, and finding new algorithms to tackle them more efficiently remains an outstanding challenge. Over the last two decades, quantum optimisation has attracted attention as a potential route towards achieving computational speedups for certain problems [2]. Quantum optimisation approaches rely on preparing a many-body quantum system in a state that encodes the solution of the combinatorial optimisation problem at hand. Typically, this state preparation is achieved through quantum annealing algorithms (QAA) [3, 4] that rely on the quantum adiabatic principle, or using hybrid quantum-classical approaches [5, 6] such as the Variational Quantum Eigensolver (VQE) [7–10] or Quantum Approximate optimisation Algorithms (QAOA) [11–15]. These approaches are particularly well suited for combinatorial optimisation problems that admit formulations as spin models, with examples including maximum (weighted) independent set (MIS/MWIS) problems, and quadratic unconstrained binary optimisation (QUBO) [16].

Due to their ability to realize programmable spin models, neutral atom quantum computers have recently emerged as a particularly promising platform for quantum optimisation [17, 18]. In these systems, the Rydberg blockade mechanism naturally mimics the graph problem’s independence constraint, resulting in a native embedding of the MIS problem on a particular family of geometrical graphs called unit-disk graphs (UDGs) [19, 20]. The use of QAA to solve the MIS problem on UDGs with King’s connectivity formed by hundreds of atoms has been experimentally demonstrated recently [21, 22], with

an indication towards a superlinear quantum speedup for hard graph instances. However, subsequent work [23] showed that MIS instances on UDGs with King’s connectivity can be optimally solved for up to thousands of nodes within minutes by classical approaches (custom or generic commercial solvers) on commodity hardware, without instance-specific fine-tuning. This result highlights the importance of extending the range of problems that can be embedded in neutral atom arrays beyond UDG-MIS, not only to widen the scope of possible real-world applications of this technology but also to identify instances of quantum advantage. In this spirit, several proposals have been put forward to map non-UDG MIS [24–26], QUBO [27], higher-order unconstrained binary optimisation (HUBO) [28], satisfiability [29] and general combinatorial optimisation [30] problems onto the UDG-MIS problem using ancillary atoms, and requiring only global control.

Another possibility to encode problems beyond UDG-MIS in neutral atom hardware is to use local control fields [31]. This enables the realisation of differential weights in the vertices represented by the atoms, permitting the embedding of MWIS problems defined on UDGs [32]. Importantly, UDG-MWIS problems can further be mapped into more general combinatorial optimisation problems such as non-UDG MWIS, QUBO or integer factorisation using an approach based on modular gadgets to copy and delocalise the information of the logical variables, and create arbitrary non-local interactions [33, 34]. Alternatively, an implementation based on the parity architecture [35] allows conversion of QUBO and HUBO problems into UDG-MWIS [36]. Both of these approaches require at worst a $\mathcal{O}(N^2)$ overhead for a problem with N logical variables, significantly reducing the ancillary qubit count from $\mathcal{O}(N^6)$ of previous proposals using only global addressing [21]. However, while there are recent proposals to optimize the layout of the embedded graphs [37], the overhead required for the known mappings into UDG-MWIS still poses a challenge for the embedding of large-scale combinatorial optimisation problems onto

* These authors contributed equally to this work.

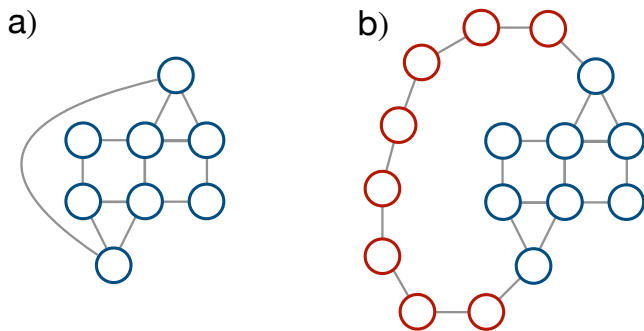


FIG. 1. (a) Example of MWIS problem defined on a graph with non-unit-disk connectivity. (b) Embedding of the graph shown in (a) into a layout compatible with the neutral atom architecture using a quantum wire, with the atoms forming it represented by red circle.

near-term neutral atom hardware.

In this paper, we introduce a hardware-efficient scheme to map non-UDG MWIS and QUBO problems into a MWIS problem defined on a UDG. Our approach is based on chains of atoms in the blockade regime, which we will call *quantum wires*, to mediate interactions between physically separated vertices, schematically shown in Fig. 1. For problems that can be formulated on graphs with quasi-UDG connectivity, and which require only a handful of long-range interactions, this allows to significantly lower the overhead in ancillary atoms with respect to the general embedding schemes discussed above. By engineering the weights of the atoms forming the wires, we further ensure the preservation of the spectrum of the original problem. This goes beyond the wire architecture presented in [24, 25], which is designed to encode unweighted problems and also only preserves the ground state, requiring post-selection of the anti-ferromagnetic state of the wires to identify valid solutions. Our wire constructions rely only on the blockade condition being fulfilled between neighbouring atoms, easing the experimental requirements with respect to proposals that require precise control of the relative strength of the interactions [31, 38].

The rest of the paper is organized as follows. In Sec. II we review the implementation of UDG-MWIS problems on neutral atom hardware. Section III introduces wire constructions that allow for the encoding of MWIS problems on non-UDG geometries, while Sec. IV explains how these wires can be adapted to encode QUBO problems as UDG-MWIS. Sec. V presents examples of non-UDG MWIS and QUBO problems embedded into UDG-MWIS using these wires, and we perform simulations of quantum annealing protocols to showcase the feasibility of this approach. In Sec. VI we analyse the performance of the annealing protocol by studying the scaling of the minimal energy gap along the adiabatic path with the wire length, and further probe the robustness of the embedding scheme against variations of the vertex weights. We conclude in Sec. VII with a summary of our results, and

an outlook for future work.

II. BACKGROUND

A weighted graph $G(V, E)$ consists of a set of vertices V , each with weight $w_i > 0$, and a collection of edges E between pairs of vertices. The Maximum Weighted Independent Set (MWIS) is defined as the subset of vertices not connected by an edge that maximizes the total sum of the weights. Introducing binary variables $n_i = \{0, 1\}$ to indicate whether vertex i belongs to the set, we can identify the MWIS with the bitstring $\{n_i\}$ that minimises the following classical cost function

$$H_{\text{MWIS}} = - \sum_i w_i n_i + \sum_{(i,j) \in E} U_{ij} n_i n_j, \quad (1)$$

where $U_{ij} > \max\{w_k\}$ is an energy penalty that ensures that no two vertices connected by an edge belong simultaneously to the MWIS. Let us also consider a Unit Disk Graph (UDG), which is graph that can be embedded in a two-dimensional plane and such that there is an edge between two vertices i and j if and only if their separation fulfills the condition $r_{ij} < R$, where R is the so-called unit disk radius. The cost function of the UDG-MWIS problem, i.e. the MWIS problem defined on UDG graphs, can be naturally mapped to the many-body Hamiltonian of a neutral atom array with a laser driving between a ground state $|g\rangle \equiv |0\rangle$ and a Rydberg state $|r\rangle \equiv |1\rangle$

$$H_{\text{Ryd}}/\hbar = \frac{\Omega}{2} \sum_i \sigma_i^x - \sum_i \Delta_i n_i + \sum_{i < j} V(r_{ij}) n_i n_j, \quad (2)$$

where Ω is the Rabi frequency, Δ_i is a site-dependent detuning from the $|0\rangle \leftrightarrow |1\rangle$ transition frequency, $n_i \equiv |1\rangle_i \langle 1|$ is an operator that counts the number of Rydberg excitation on site i , and $V(r) = C_6/r^6$ is the dipole-dipole van der Waals (vdW) interaction strength between two atoms separated a distance r . Because of this interaction, each atom has a blockade radius $r_B^i = \sqrt[6]{C_6/\sqrt{\Omega^2 + \Delta_i^2}}$ in which only one excitation can occur. In the limit $\Omega = 0$, defining the smallest blockade radius as $r_B^{\min} = \sqrt[6]{C_6/\max\{\Delta_i\}}$ and assuming $V(r > r_B^{\min}) \approx 0$, the ground state of H_{Ryd} encodes the solution of a UDG-MWIS problem with weights $0 \leq \tilde{w}_i = \Delta_i/\Delta_0 \leq 1$, and unit disk radius $R \approx r_B^{\min}$, realizing the constraint $V(r_{ij}) > \max\{\Delta_k\}$ for all (i, j) sharing an edge. Here, the maximum detuning $\Delta_0 = 0.9C_6/R^6$ is chosen to ensure the blockade constraints between atoms that are connected by an edge. Although the assumption $V(r > r_B) \approx 0$ is well justified due to the rapid decay of the dipole interactions with the atom separation, in practical implementations the interaction tails can have a non-negligible effect on the ground state of the system. Therefore, it is necessary to further impose the condition that the maximal unwanted interaction is less than the smallest weight in the problem, $\max_{(i,j) \in E} V(r_{ij}) < \min_k \Delta_k$. This

guarantees that all pairs of vertices not connected by an edge are allowed to belong to the MWIS.

This correspondence between H_{MWIS} and H_{Ryd} opens up the possibility to solve combinatorial optimisation tasks via embedding the UDG-MWIS problem by annealing a neutral atom array into the ground state configuration of interest. In this work, we simulate this process using the annealing protocol introduced in [32]. This protocol is defined in terms of a global Rabi frequency $\Omega(t)$ and local detuning pulses $\Delta_i(t) = \Delta(t) + \delta_{AC}^i(t)$, where $\Delta(t)$ is the global detuning of the Rydberg lasers and $\delta_{AC}^i(t) = \tilde{w}_i \delta_{AC}(t)$ are local AC light shifts which are holographically projected onto the atoms using a Spatial Light Modulator (SLM). Initially, the laser parameters are initialised at $\Omega = 0$ and $\Delta_i = \Delta < 0$, with the atom prepared in the corresponding ground state $|0\rangle^{\otimes N}$. In the first part of the sequence, the Rabi frequency $\Omega(t)$ is ramped up to its maximum value, and the detuning is uniformly increased by controlling the global control field $\Delta(t)$ until hitting resonance for all the atoms, $\Delta_i = \Delta = 0$. After crossing resonance, the global Rabi frequency $\Omega(t)$ is kept constant, and local detunings $\Delta_i(t) = \delta_{AC}^i(t) = \tilde{w}_i \delta_{AC}(t)$ are introduced for every atom while keeping the global Rydberg lasers at resonance $\Delta = 0$. Finally, after reaching sufficiently high detunings to ensure the blockade constraints between atoms connected by an edge, the Rabi frequency is turned down to $\Omega = 0$ so that the final Hamiltonian has a direct correspondence with the classical MWIS cost function in Eq. (1).

This annealing protocol or similar ones [34] can also be used to solve more general optimisation problems such as MWIS with arbitrary connectivity, quadratic (and higher order) unconstrained binary optimisation problems (QUBO and HUBO) or integer factorisation [27, 28, 30, 33, 36, 39]. In these cases, it is necessary to first map the problem into a UDG-MWIS, prepare the ground state of the resulting weighted graph using a neutral atom quantum computer, and finally undo the mapping to read out the solution of the original problem. Recently, systematic recipes were introduced to realise these mappings between general optimisation problems and UDG-MWIS. Ref. [33] introduces gadgets on an atom grid that allows for the realisation of arbitrary connections between vertices, while Refs. [30, 36] map the problem onto the parity architecture using constraints. All of these approaches have the advantage of working for general graphs, but require $\sim N^2$ physical qubits to implement logical problems of N binary variables, introducing an overhead that makes the practical implementation of large-scale combinatorial problems on current neutral atom hardware challenging. Here, we show that for MWIS and QUBO problems with quasi-UDG connectivity, i.e. graphs for which most edges can be represented in a UDG except for a few long-range interactions, the ancillary atom count can be drastically reduced by using quantum wires. Similar approaches for MIS have been considered in [24, 25, 38]. Here, we build on this, proposing weighted atomic wires

that do not require post-selection to identify correct solutions, and which preserve the spectrum of the original problem.

III. QUANTUM WIRES FOR MWIS PROBLEMS

Fig. 2 (a) illustrates a basic wire construction to realise an MWIS constraint between two physically separated vertices with weights α and β (with $\alpha > \beta$ in this example). The allowed configurations in the logical MWIS problem are $|\alpha, \beta\rangle = \{|10\rangle, |01\rangle, |00\rangle\}$, with corresponding energies $\{-\alpha, -\beta, 0\}$. The wire consists of an even number of atoms L with a uniform weight c , arranged in such a way that every atom is within the blockade radius of its two neighbours, forming an effective one-dimensional chain. As shown in the energy diagram in Fig. 2 (a), choosing ancilla weights $c > \alpha + \beta$ yields the correct ordering of the states of the logical nodes in the three lowest-energy configurations of the system formed by the logical nodes and the wire, with the logical state $|11\rangle$ being energetically forbidden. Even though we only show one possible configuration for the $|00\rangle$ and $|11\rangle$ states, we note that, without considering the effect of vdW interactions, they have respectively degeneracies of $L/2 + 1$ and $L/2$ due to the degree of freedom corresponding to the localization of the domain wall [34]. All the states of the wire are shifted by a constant offset $-Lc/2$ with respect to their corresponding logical configurations, ensuring the preservation of the MWIS solution when the wire is embedded in a larger graph with more atoms. We emphasize that this construction *preserves* the spectrum of the logical problem, and truly facilitates an interaction between physically spatially separated nodes.

The construction that enables us to realise an edge between two spatially separated weighted atoms can also be generalised to delocalise other connectivity structures involving a larger number of atoms. In Fig. 2 (b) we illustrate a wire construction that realises an all-to-all connectivity between three atoms with weights α, β and γ , where atoms α and β are within the blockade radius of each other but outside the one of atom γ . The wire is constructed in the same way as in Fig. 2 (b), but now with vertices α and β connected to one end of the wire, and node γ to the opposite end. The analysis of the possible configurations of the wire shows that in order to preserve the correct ordering of the energy spectrum, one can choose a weight for the ancillary atom of $c > \max\{\alpha, \beta\} + \gamma$. Similarly, in Fig. 2 (c) we show how to use a wire of even length L to stretch an all-to-all connected square formed by four atoms with weights α, β, γ and δ into two separated regions, in one of which there is a direct edge between α and β and in the other an edge between γ and δ . In this situation a choice of the wire weight $c > \max\{\alpha, \beta\} + \max\{\gamma, \delta\}$ ensures the preservation of the logical spectrum. This pattern can be generalised to larger all-to-all connected structures.

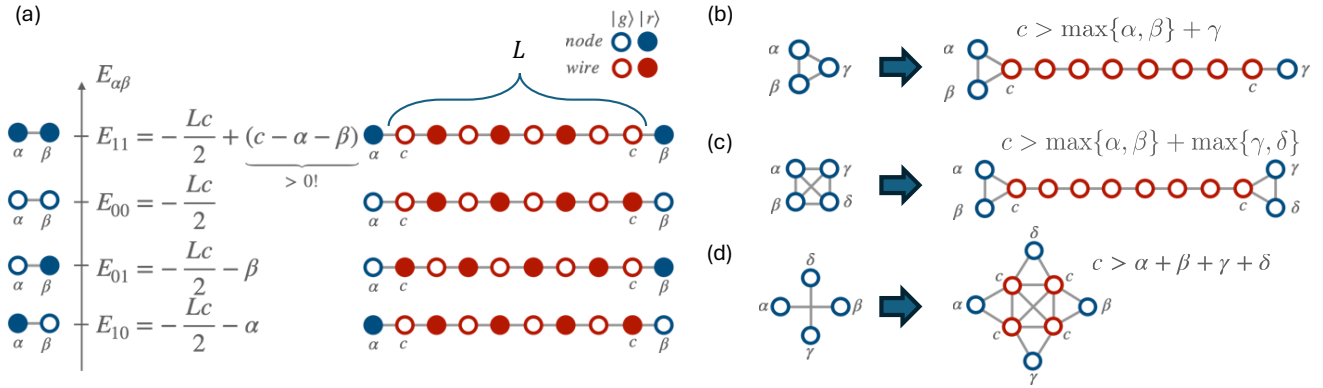


FIG. 2. (a) Basic construction of a wire to connect two nodes with weights α and β in MWIS and QUBO problems. The energy diagram shows the ordering of the eigenstates for an MWIS implementation. (b, c) Wire constructions to delocalise triangular and all-to-all square interactions between vertices in MWIS problems. (d) Generalisation of the crossing gadget introduced in [33] to allow for arbitrary weights of the nodes.

In order to implement more complicated structures with long-range connectivity it might be necessary for quantum wires to cross. This can be achieved with a generalisation of the crossing gadget introduced in Ref. [33], as shown in Fig. 2 (d). In the most general case in which the four vertices involved in the crossing have different weights $\alpha, \beta, \gamma, \delta$, choosing the weight of the crossing gadget ancillary nodes as $c > \alpha + \beta + \gamma + \delta$ guarantees the preservation of the spectrum of the logical problem.

IV. QUANTUM WIRES FOR QUBO PROBLEMS

Quadratic Unconstrained Binary Optimisation (QUBO) is a well-known NP-Hard problem with a myriad of applications. The solution of a QUBO problem can be formulated in terms of a bitstring $\{n_i\}$, with $n_i \in \{0, 1\}$ that minimizes the classical cost function

$$H_{\text{QUBO}} = \sum_i h_i n_i + \sum_{i,j} J_{ij} n_i n_j, \quad (3)$$

where h_i and J_{ij} are arbitrary coefficients. In the case when $h_i = -|h_i| < 0 \forall i$ and $J_{ij} > 0 \forall (i, j)$, H_{QUBO} can be implemented within the quantum wire framework presented here. To understand this, let us consider the simplest case of a QUBO problem defined over two variables described by the cost function

$$f(n_1, n_2) = -|h_1|n_1 - |h_2|n_2 + J_{12}n_1n_2. \quad (4)$$

Comparing this expression with the wire spectrum shown in Fig. 2 (a), we can see that by choosing $\alpha = |h_1|$, $\beta = |h_2|$ and $c = J_{12}$ the states of the wire exactly mimic the QUBO cost function Eq. (4) up to a constant energy offset $-Lc/2$ (for $L \geq 2$). Note that the constraint $c > \alpha + \beta$, necessary for the MWIS implementation, is now relaxed so the state $|11\rangle$ can appear in any order in the spectrum depending on the value of J_{12} .

Following this basic construction for a 2-bit QUBO, larger problems can be implemented by assigning an atom with relative weight $w_i = h_i$ to each logical variable n_i , and connecting the logical qubits with wires with homogeneous weights $c_{ij} = J_{ij}$. The building blocks, shown in Figs. 2 (b) and (c), could also be used for triangles or squares with uniform J couplings, and the crossing gadget of Fig. 2 (d) could be used in the same way as for MWIS problems. While this approach for embedding QUBO problems is only scalable for instances with mostly local connectivity, in these scenarios it can provide an overhead reduction with respect to the proposals in Refs [27, 33, 36], which are designed for general graphs.

V. QUANTUM ANNEALING RESULTS

In this section we provide concrete examples to illustrate the procedures described in Sec. III and IV to formulate MWIS and QUBO problems as UDG-MWIS readily implementable on neutral atoms in tweezer arrays. We also simulate the annealing protocol to prepare the ground state of the resulting embeddings, obtaining high probabilities of measuring the target state even in the presence of dissipation. For the implementation of the mapped UDG graphs, we consider Cs atoms, and an encoding of the qubits in the states $|0\rangle = |6S_{1/2}, f = 4, m_f = 0\rangle$, and $|1\rangle = |80S_{1/2}, m_j = 1/2\rangle$. The two states are coupled via a two-photon transition through the intermediate state $|e\rangle = |7P_{1/2}\rangle$, which is resolved into its hyperfine components and far off-resonance at center of mass detuning $\delta/2\pi = 5$ GHz. We consider a standard separation $d = 8 \mu\text{m}$ between the atoms, for which the van der Waals interaction strength is $C_6/d^6 = 2\pi \times 12.29$ MHz [40]. Time evolution is simulated using the effective model described in [41], which accounts for dissipation from the intermediate state involved in the two-photon excitation from $|0\rangle$ to $|1\rangle$, and the finite lifetime of the Rydberg state.

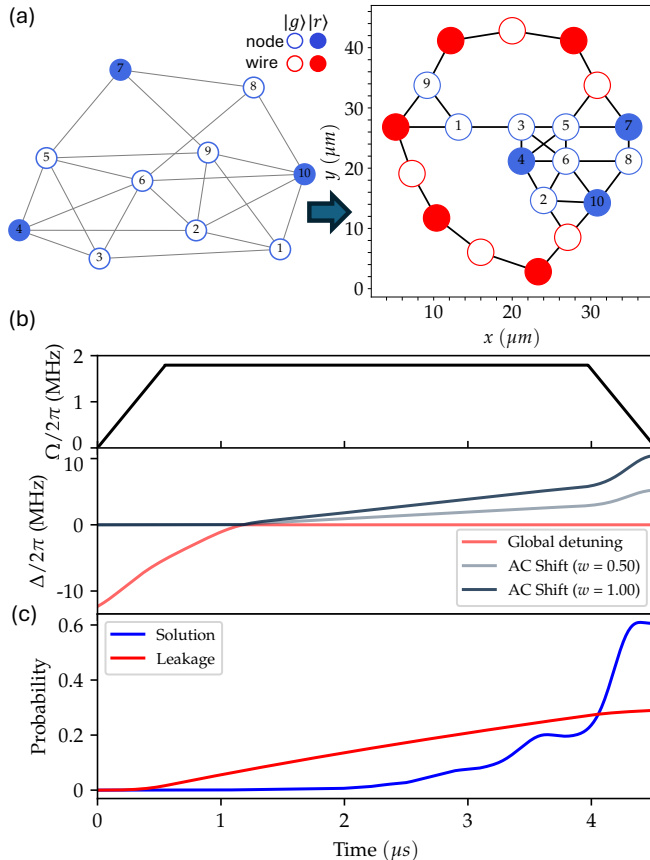


FIG. 3. (a) Graph with non-UDG connectivity over which MWIS problem is defined (left) and mapped graph with UDG connectivity (right). Blue vertices belong to the logical problem, while red ones are used for the wires. Filled circles indicate vertices that belong to the MWIS solution. (b) Annealing pulse used to drive the atom array shown on the right side of (a) into the state encoding the MWIS solution. (c) Time evolution under the pulse shown in (b) of obtaining the MWIS solution upon measuring the state of the atom array (blue line) and of leakage of the many-body wave function outside of the computational basis due to dissipation (red line).

Dissipation from $|0\rangle$ and $|1\rangle$ is assumed to be outside the computational basis. The effective damping rate from the $|1\rangle$ state is constant at $\Gamma_1/2\pi = 5.93 \times 10^{-4}$ MHz, while the effective damping rate from $|0\rangle$ is scaled proportional to $\Omega(t)^2$ to account for scattering from the intermediate state, with a peak value of $\Gamma_0/2\pi = 8.58 \times 10^{-4}$ MHz.

A. MWIS example

The problem graph for which we want to solve the MWIS problem is shown in the left part of Fig. 3 (a). By rearranging the positions of the nodes, all the edges can be made to satisfy the UDG criterion except for the triangle between nodes $\{5, 7, 9\}$, and the all-to-all connected cluster formed by nodes $\{1, 2, 9, 10\}$. As shown

Embedding vertex	w_i	\tilde{w}_i
1	56	0.362
2	67	0.434
3	47	0.304
4	87	0.563
5	78	0.508
6	99	0.641
7	81	0.524
8	51	0.330
9	71	0.459
10	82	0.531
1-2-9-10 wire	-	0.993
5-7-9 wire	-	1.000

TABLE I. Weights of the example problem graph and the corresponding mapped UDG shown in Fig. 3 (a).

in the right plot of Fig. 3 (a), these links can be realized with quantum wire constructions, resulting in an embedded graph formed by a total of 20 atoms with exclusively UDG connectivity. For comparison, we note that the implementation of the same logical problem using the gadget encoding described in [33] with additional optimisation takes a total of 211 atoms using the open software package `UnitDiskMapping.jl` [42]. Naturally, this could be further optimised, for example using graph reduction techniques [37], but for quasi-UD graphs our technique provides a robust and efficient alternative.

The weights of the original problem, shown in Table I, are integers picked randomly from the interval $[30, 100]$ with uniform probability. This range of weights has been chosen to ensure that the largest unwanted van der Waals interaction is not larger than the smallest weight. The filled blue nodes in the left part of Fig. 3 (a) form the MWIS of the logical graph. In the mapped graph, the weights of the upper and lower wires are chosen as $w_9 + \max\{w_5, w_7\}$, and $\max\{w_1, w_9\} + \max\{w_2, w_{10}\}$ respectively. For convenience, all weights are subsequently normalised to a maximum value of 1, such that $0 < \tilde{w}_i \leq 1$. In this way, the maximum detuning at each site is given by $\Delta_i = \tilde{w}_i \Delta_0$, with $\Delta_0 = 0.9C_6/d^6$. The ground state of the embedded graph, depicted in the right part of Fig. 3 (a) with blue (red) filled circles for logical (ancillary) atoms in the Rydberg state coincides with the solution of the logical MWIS problem.

Fig. 3 (b) shows the $\Omega(t)$ and $\Delta_i(t)$ annealing pulses used to prepare the ground state of (2) for the mapped graph shown in Fig. 3 (a). The Rabi frequency (upper panel) is linearly ramped up to its maximum value, kept constant to enable transitions to the Rydberg manifold, and linearly ramped down at the end of the sequence. The detuning is parametrized by using the Variational Quantum Adiabatic Ansatz (VQAA) [21] consisting of three linear segments that are smoothed out at the intersection points. The pulse has been optimized on a reduced graph without wires encoding the original MWIS problem, and then run on the full UDG-MWIS embedded graph. Fig. 3 (c) shows the evolution of both the target state probability, and leakage outside of the computa-

tional basis along the annealing path. The target state probability is given by tracing out the ancillary atoms in the ground state population shown in Fig. 3 (a). At the end of the pulse sequence we obtain a probability of $\sim 60\%$ of measuring the correct solution to the MWIS problem, in spite of the fact that there is a $\sim 29\%$ probability of the state decaying outside of the computational basis. These results are very encouraging as this means that, on average, in an experimental implementation of the protocol it would suffice to run the annealing protocol $1/0.60 \sim 1.6$ times in order to measure a bitstring that contains the solution of the logical problem.

B. QUBO examples

In order to illustrate the use of quantum wires to embed QUBO problems in neutral atom arrays, we start by considering a simple instance consisting of 4 binary variables with local fields $\{h_1, h_2, h_3, h_4\}$ and interactions $\{J_{1,2}, J_{1,4}, J_{3,4}\}$, with values gathered in the first column of Table II. As shown in Fig. 4 (a), the interactions occurring in this problem can be represented as a one-dimensional (1D) chain. Therefore, the embedding in a neutral atom array can be achieved by adding two wire atoms in between each atom representing a logical variable. This is shown in Fig. 4 (a), where blue and red circles represent logical nodes and wire atoms respectively. As in the MWIS example discussed previously, the weights of the embedded 1D QUBO graph, which are collected in the third column of Table II, are renormalised to a maximum value of 1 for convenience. The filled circles indicate the MWIS solution of the embedded graph, which coincides with the solution of the logical QUBO problem. The annealing ramp that we use to prepare the ground state, which is shown in Fig. 4 (b), has been found by taking as an initial ansatz the pulse used for the MWIS example and re-optimising. As shown in Fig. 4 (c), at the end of the sequence we find a probability of $\sim 82\%$ of measuring the correct solution (after tracing out the state of the wires), with a probability of leakage outside of the computational basis of $\sim 18\%$.

To showcase the implementation of a more complex QUBO problem, we add the terms $\{J_{1,3}, J_{2,3}, J_{2,4}\}$ into the example 1D problem with the values shown in the first column of Table II. As displayed in Fig. 4 (b), the resulting interactions of the QUBO problem can now be represented as an all-to-all (ATA) connected square. As a result of this, the embedding in neutral atom hardware requires a crossing gadget to allow for independent wires mediating the 1-2 and 3-4 interactions, and the total atom count of the embedding goes up to 28 due to the need to use longer wires in the outer connections to avoid unwanted interactions. Nevertheless, this overhead is still lower than what would be required in the schemes proposed in [33, 36]. We simulate preparation of the ground state of the embedded graph taking the same pulse as in the previous 1D QUBO example as a reference and

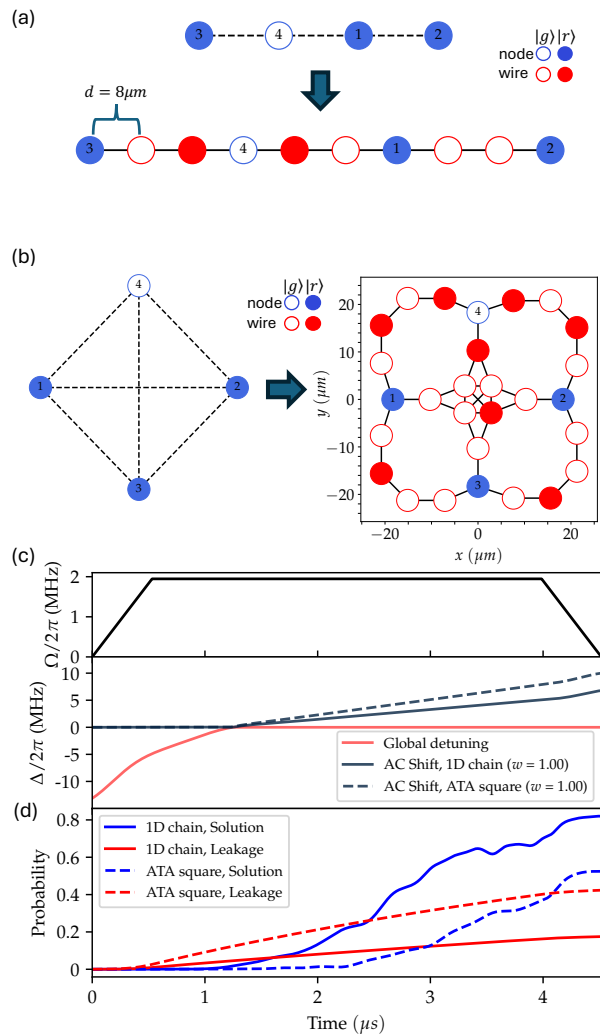


FIG. 4. (a) Logical QUBO problem (up) and corresponding embedding in a 1D chain using quantum wires (down). (b) Extension of the QUBO problem from (a) resulting in an ATA connected square (left) and corresponding embedding in a weighted UDG (right). In (a) and (b) blue vertices belong to the logical problem, while red ones are used for the wires. Filled circles indicate vertices that belong to the QUBO solution. (c) Annealing pulse used to drive the atom arrays shown in (a) and (b) into their ground states encoding the solution of the corresponding QUBO problems. (d) Time evolution under the pulse shown in (c) of obtaining the QUBO solution upon measuring the state of the atom array (blue lines) and of leakage of the many-body wave function outside of the computational basis due to dissipation (red lines). Solid (dashed) lines correspond to the 1D (ATA square) graph shown in (a) ((b)).

slightly increasing the detuning at the end of the ramp, as shown in Fig. 4 (c). As can be seen in Fig. 4 (d), this preparation sequence results in a probability of $\sim 52\%$ of measuring a state representing the solution of the logical QUBO problem, in spite of a leakage of $\sim 42\%$ of the total probability outside of the computational basis.

QUBO parameter	Embedding vertex	\tilde{w}_i (1D chain)	\tilde{w}_i (ATA square)
$h_1 = -12$	1	0.750	0.429
$h_2 = -15$	2	0.938	0.536
$h_3 = -16$	3	1.000	0.571
$h_4 = -9$	4	0.563	0.321
$J_{1,2} = 2$	wire 1-2	0.125	0.071
$J_{1,3} = 8$	wire 1-3	-	0.286
$J_{1,4} = 11$	wire 1-4	0.688	0.393
$J_{2,3} = 6$	wire 2-3	-	0.214
$J_{2,4} = 8$	wire 2-4	-	0.286
$J_{3,4} = 12$	wire 3-4	0.313	0.429
-	Crossing gadget	-	1.000

TABLE II. Weights and interaction strengths of the example QUBO problems and the corresponding mapped UDGs shown in Fig. 4 (a) and (b).

These figures could likely be improved with a full pulse re-optimisation.

VI. ROBUSTNESS OF THE WIRE ARCHITECTURE

While the proposed wire architecture is guaranteed to give the correct groundstate solution, it is *a priori* not clear how robust the annealing ramps and the embedding scheme are to experimental imperfections and uncertainties. In this section we want to separately consider two aspects of this - (1) how robust and scalable is the annealing performance of the quantum wire as the system sizes is increased, and (2) how resilient is the embedding to variations in the vertex weights

A. The annealing protocol

As indicated by the results discussed above, the quantum wire approach presented here allows for a flexible and robust encoding of combinatorial optimisation problems that are close to UDG connectivity. In order to better understand the reason for this robustness, we numerically compute the spectral gap of the basic building blocks in this architecture as a function of system size. The top panel of Fig. 5 shows the spectral gap $\Delta E(t)$ of the Rydberg Hamiltonian Eq. 2 along the annealing path for logical wire weightings $(\alpha, \beta) = \{(0.7, 0.3), (0.51, 0.5)\}$ in (a) and (b) respectively. The different shadings indicate the system size (logical and ancilla atoms) of the wire $N = 2^k$ for $2 \leq k \leq 9$. The minimal spectral gap ΔE_{\min} along the path is marked by black crosses for each system size. We used the same annealing schedule for all considered logical weights. It has been variationally optimised for the smallest $N = 4$ wire with logical weights $(0.7, 0.3)$ to isolate the effect of the wire length on the spectral gap. Using the matrix product state (MPS) ansatz, we variationally find the spectral gap using the density matrix

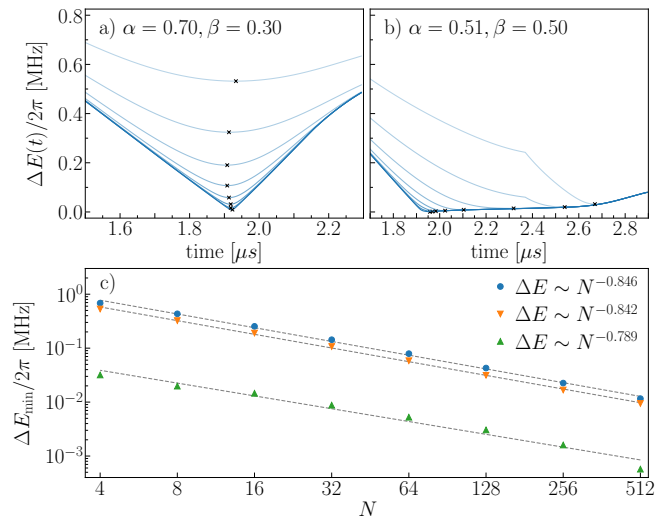


FIG. 5. The top plots show the spectral gap along the annealing path $\Delta E(t)$ for different system sizes $N = \{4, \dots, 512\}$ (light to dark blue) for wire weights $(\alpha, \beta) = (0.7, 0.3)$ (a) and $(\alpha, \beta) = (0.51, 0.5)$ (b). The black markers indicate the extracted minimum spectral gap depicted in the main plot. (c) Minimal spectral gap ΔE_{\min} as a function of system size for wire weightings $(\alpha, \beta) = \{(0.1, 0.9), (0.7, 0.3), (0.51, 0.5)\}$ (blue circle, orange inverted triangle, and green triangle respectively). The spectral gap closes polynomially with system size $\sim N^{-z}$, with a linear fit giving an exponent of $z \lesssim 1$. These results were obtained using DMRG simulations using a bond dimension of $D = 200$, a truncation error of $\epsilon = 10^{-12}$. The extracted energies were converged to a threshold of 10^{-4} .

renormalization group (DMRG) algorithm [43–47]. The bottom plot of Fig. 5 (c) shows the minimum spectral gap (as indicated by the black markers in the top plots) as a function of system size N for different wire weights. For the wires, we find that the spectral gap closes polynomially as N^{-z} with $z \lesssim 1$, indicating that these wires do not pose a fundamental problem for the adiabatic protocol. These findings are also in agreement with the recent analysis performed in Ref. [34].

The black markers in Fig. 5 (a) and (b) indicate where the minimal spectral gap occurs along the annealing path. We have chosen two distinct scenarios of a strongly imbalanced (a) and a closely balanced (b) wire. We already saw above that the spectral gap closes more slowly (smaller z) for the former case (a). Interestingly, in this case the minimum gap appears to occur around the same detuning value, independent of the wire length. Meanwhile for the closely balanced wire (b) the gap closes more quickly with system size, and there is a larger variation in the place where the minimal gap occurs along the annealing path. This is intuitively expected as the MWIS problem is computationally more difficult if the weights are all very similar due to smaller energy gaps between the different configurations. We obtain qualitatively very similar results for the triangle and square constructions of Fig. 2 (b-c) with a scaling exponent of $z \lesssim 1.5$.

B. Robustness of a single quantum wire

In order to evaluate how robust the embedding scheme is to shot-to-shot fluctuations in the applied local light shifts, we isolate a single wire module, and vary the local detunings randomly. For concreteness we draw the random weights from a normal distribution centered around the ideal detuning value, and study how these deviations from the ideal implementation can affect the low-energy spectrum of the quantum wire. Let X be a random variable $X \sim \mathcal{N}(\mu_X, \sigma_X^2)$, where $\mu_X = \{\alpha, \beta, c\}$, and $\sigma_X = \{\sigma_\alpha, \sigma_\beta, \sigma_c\}$ respectively. The configurational energies of the wire are thus also random variables, and specifically the distributions of the low-energy states shown in Fig. 2 (a) are given by $E_{x_\alpha, x_\beta} \sim \mathcal{N}(\mu_{x_\alpha, x_\beta}, \sigma_{x_\alpha, x_\beta}^2)$, with

$$\mu_{x_\alpha, x_\beta} = -\alpha x_\alpha - \beta x_\beta - c N_{x_\alpha, x_\beta}, \quad (5)$$

$$\sigma_{x_\alpha, x_\beta}^2 = x_\alpha \sigma_\alpha^2 + x_\beta \sigma_\beta^2 + N_{x_\alpha, x_\beta} \sigma_c^2, \quad (6)$$

their mean and variance respectively. Here $x_i \in \{0, 1\}$ indicates the absence (presence) of an excitation on either end of the wire (α or β respectively), and $N_{x_\alpha, x_\beta} = (L - 2x_\alpha x_\beta)/2$ is the total number of excitations on the ancilla atoms for the considered states. The expectation values of the energies coincide with the ideal wire result as expected, and we note that fluctuations in the detunings lead to a standard deviation $\sigma = \sqrt{\sigma_\alpha^2 + \sigma_\beta^2 + L\sigma_c^2}$ which scales as $\sigma \sim \sqrt{L}$ with increasing wire length. We also note that this analysis holds both considering only UDG interactions and van der Waals (vdW) tails, as in the latter case the long-range interactions are identical in the lowest two energy configurations.

We test empirically the robustness of a single wire to noise in the local light shifts by setting the ground state with $\alpha > \beta$, randomizing the weights of the logical nodes and the wire atoms in the manner discussed above and checking whether the new ground state still corresponds to the 10 state. To speed up the calculations, we only evaluate the energies of the $L+3$ configurations of the system formed by the logical nodes and the wire that respect the blockade constraint. In Fig. 6 (a) and (b) we show respectively the results corresponding to $\alpha = 0.6, \beta = 0.4$ and $\alpha = 0.8, \beta = 0.2$ for wires of different lengths L and for different values of the standard deviation σ_X of the noise Gaussian, which for each atom is chosen such that μ_X/σ_X is constant across the system. Each data point has been obtained by sampling 100,000 random local detuning realizations. The success probability is larger for the case $\alpha = 0.8, \beta = 0.2$ shown in Fig. 6 (a) than for the case $\alpha = 0.6, \beta = 0.4$ of Fig. 6 (b). This is to be expected from Eq. (5), as the expectation value of the gap between the $|10\rangle$ and the rest of states is larger for $\alpha = 0.8, \beta = 0.2$ than for $\alpha = 0.6, \beta = 0.4$. Even though there is a decay in the probability of successfully encoding the solution of the MWIS problem with increasing values of the standard deviation σ_X and the wire length L , for lengths of

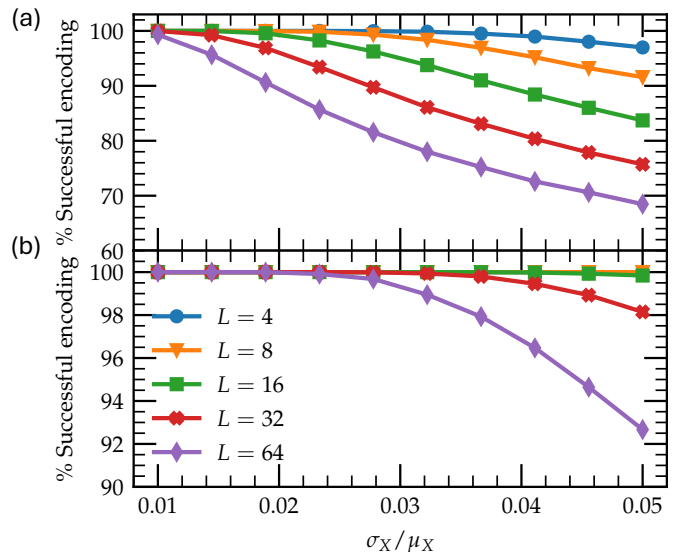


FIG. 6. Probability of successfully encoding the ground state in the presence of Gaussian fluctuations in the local light shift for wires of different length L as a function of the standard deviation σ_X of the distribution. Plot (a) corresponds to the choice of weights $\alpha = 0.6, \beta = 0.4$, and (b) $\alpha = 0.8, \beta = 0.2$. Each data point has been estimated by sampling across 100,000 random realizations of the local light shifts.

up to $L = 64$ and standard deviation $\sigma_X/\mu_X = 0.05$ the success probability remains lower-bounded by $\sim 70\%$ in the case $\alpha = 0.6, \beta = 0.4$ and by $\sim 92\%$ for $\alpha = 0.8, \beta = 0.2$. When the wire is embedded in a larger graph, we expect the robustness of the encoding to be enhanced by the additional gaps induced by the structure of the logical problem and the presence of residual long-range vdW interactions.

VII. CONCLUSION

In this paper, we proposed a novel quantum wire architecture to map certain hard combinatorial optimisation problems on general graphs to a UDG-MWIS problem. This quantum wire encoding serves as a building block for solving optimisation problems on neutral atom quantum processors, allowing for an efficient encoding and greater flexibility in problem graphs that can be solved using this technology.

We demonstrated how our quantum wire scheme is able to efficiently encode MWIS problems beyond the UDG connectivity by mediating effective interactions between distant vertices. Furthermore, by carefully tuning the weights of the ancillary wire atoms, we are able to faithfully preserve, and tune the entire logical spectrum of the target problem which allows for successful encodings of QUBO problems within the same architecture. Because we do not encode a single qubit in the entire wire, but

rather we use it to facilitate long-range connections between distant nodes, we find that, relative to previous general schemes [33, 36], our protocol requires substantially fewer resources.

We numerically investigated the robustness of the wire architecture by looking at the scaling of the minimum spectral gap along the annealing path for the wire module, and also by studying the effect of experimental disorder on the local light shifts. We found that the size of the gap has a polynomial scaling with system size and that the wire encoding is robust to fluctuations in the local detunings. We provided numerical simulations of realistic quantum annealing ramps, finding high success probabilities even for moderate graph sizes and in the presence of dissipation. In this way the quantum wires introduced here represent a flexible approach to go beyond UDG-MWIS problems, and open up a way to target more complex combinatorial optimisation problems.

Finally, we note that while we discuss this embedding scheme from a physical implementation perspective, it

can also be used as a sub-routine for classical solvers to efficiently map non-UDG graphs into weighted UDG problem instances. An intriguing direction for future work is the optimisation and automatism of the embedding layout, as well as the potential integration of the wire architecture with existing toolkits for the reduction of MWIS problems and the identification of hard instances that require the implementation of quantum solutions [37].

VIII. ACKNOWLEDGEMENTS

This work was supported by EPSRC through grant number EP/Y005058/2 and by Innovate UK through the Innovation Accelerator for Neutral Atom Quantum Optimisation (Grant No. 10059444), as well as the EPSRC Prosperity Partnership *SQuAre* (Grant No. EP/T005386/1) with funding from M Squared Lasers Ltd.

-
- [1] V. T. Paschos, *Applications of combinatorial optimization*, Vol. 3 (John Wiley & Sons, 2014).
 - [2] A. Abbas, A. Ambainis, B. Augustino, A. Bärtzsch, H. Buhrman, C. Coffrin, G. Cortiana, V. Dunjko, D. J. Egger, B. G. Elmegreen, *et al.*, *Nature Reviews Physics* **6**, 718 (2024).
 - [3] P. Hauke, H. G. Katzgraber, W. Lechner, H. Nishimori, and W. D. Oliver, *Reports on Progress in Physics* **83**, 054401 (2020).
 - [4] A. Rajak, S. Suzuki, A. Dutta, and B. K. Chakrabarti, *Philosophical Transactions of the Royal Society A* **381**, 20210417 (2023).
 - [5] M. Cerezo, A. Arrasmith, R. Babbush, S. C. Benjamin, S. Endo, K. Fujii, J. R. McClean, K. Mitarai, X. Yuan, L. Cincio, and P. J. Coles, *Nature Reviews Physics* **3**, 625 (2021).
 - [6] N. Astrakhantsev, G. Mazzola, I. Tavernelli, and G. Carleo, *Phys. Rev. Res.* **5**, 033225 (2023).
 - [7] A. Peruzzo, J. McClean, P. Shadbolt, M.-H. Yung, X.-Q. Zhou, P. J. Love, A. Aspuru-Guzik, and J. L. O'Brien, *Nature Communications* **5**, 4213 (2014).
 - [8] A. Kandala, A. Mezzacapo, K. Temme, M. Takita, M. Brink, J. M. Chow, and J. M. Gambetta, *Nature* **549**, 242 (2017).
 - [9] C. Hempel, C. Maier, J. Romero, J. McClean, T. Monz, H. Shen, P. Jurcevic, B. P. Lanyon, P. Love, R. Babbush, A. Aspuru-Guzik, R. Blatt, and C. F. Roos, *Phys. Rev. X* **8**, 031022 (2018).
 - [10] C. Kokail, C. Maier, R. van Bijnen, T. Brydges, M. K. Joshi, P. Jurcevic, C. A. Muschik, P. Silvi, R. Blatt, C. F. Roos, and P. Zoller, *Nature* **569**, 355 (2019).
 - [11] E. Farhi, J. Goldstone, and S. Gutmann, *A quantum approximate optimization algorithm* (2014), [arXiv:1411.4028 \[quant-ph\]](https://arxiv.org/abs/1411.4028).
 - [12] D. Wecker, M. B. Hastings, and M. Troyer, *Phys. Rev. A* **92**, 042303 (2015).
 - [13] J. Wurtz and P. Love, *Phys. Rev. A* **103**, 042612 (2021).
 - [14] E. Farhi, J. Goldstone, S. Gutmann, and L. Zhou, *Quantum* **6**, 759 (2022).
 - [15] K. Blekos, D. Brand, A. Ceschini, C.-H. Chou, R.-H. Li, K. Pandya, and A. Summer, *Physics Reports* **1068**, 1 (2024).
 - [16] A. Lucas, *Frontiers in physics* **2**, 5 (2014).
 - [17] L. Henriot, L. Beguin, A. Signoles, T. Lahaye, A. Browaeys, G.-O. Raymond, and C. Jurczak, *Quantum* **4**, 327 (2020).
 - [18] M. Morgado and S. Whitlock, *AVS Quantum Science* **3** (2021).
 - [19] H. Pichler, S.-T. Wang, L. Zhou, S. Choi, and M. D. Lukin, *arXiv preprint arXiv:1808.10816* (2018).
 - [20] H. Pichler, S.-T. Wang, L. Zhou, S. Choi, and M. D. Lukin, *arXiv preprint arXiv:1809.04954* (2018).
 - [21] S. Ebadi, A. Keesling, M. Cain, T. T. Wang, H. Levine, D. Bluvstein, G. Semeghini, A. Omran, J.-G. Liu, R. Samajdar, *et al.*, *Science* **376**, 1209 (2022).
 - [22] K. Kim, M. Kim, J. Park, A. Byun, and J. Ahn, *Scientific Data* **11**, 111 (2024).
 - [23] R. S. Andrist, M. J. Schuetz, P. Minssen, R. Yalovetzky, S. Chakrabarti, D. Herman, N. Kumar, G. Salton, R. Shaydulin, Y. Sun, *et al.*, *Physical Review Research* **5**, 043277 (2023).
 - [24] M. Kim, K. Kim, J. Hwang, E.-G. Moon, and J. Ahn, *Nature Physics* **18**, 755 (2022).
 - [25] A. Byun, M. Kim, and J. Ahn, *PRX Quantum* **3**, 030305 (2022).
 - [26] C. Dalyac, L.-P. Henry, M. Kim, J. Ahn, and L. Henriot, *arXiv preprint arXiv:2306.13373* (2023).
 - [27] A. Byun, J. Jung, K. Kim, M. Kim, S. Jeong, H. Jeong, and J. Ahn, *Advanced Quantum Technologies* **7**, 2300398 (2024).
 - [28] A. Byun, S. Jeong, and J. Ahn, *Physical Review A* **110**, 042612 (2024).
 - [29] S. Jeong, M. Kim, M. Hhan, J. Park, and J. Ahn, *Phys. Rev. Res.* **5**, 043037 (2023).

- [30] M. Lanthaler, K. Ender, C. Dlaska, and W. Lechner, arXiv preprint arXiv:2410.03902 (2024).
- [31] K. Goswami, R. Mukherjee, H. Ott, and P. Schmelcher, *Physical Review Research* **6**, 023031 (2024).
- [32] A. G. de Oliveira, E. Diamond-Hitchcock, D. M. Walker, M. T. Wells-Pestell, G. Pelegrí, C. J. Picken, G. P. A. Malcolm, A. J. Daley, J. Bass, and J. D. Pritchard, *PRX Quantum* **6**, 010301 (2025).
- [33] M.-T. Nguyen, J.-G. Liu, J. Wurtz, M. D. Lukin, S.-T. Wang, and H. Pichler, *PRX Quantum* **4**, 010316 (2023).
- [34] L. Bombieri, Z. Zeng, R. Tricarico, R. Lin, S. Notarnicola, M. Cain, M. D. Lukin, and H. Pichler, arXiv preprint arXiv:2411.04645 (2024).
- [35] W. Lechner, P. Hauke, and P. Zoller, *Science advances* **1**, e1500838 (2015).
- [36] M. Lanthaler, C. Dlaska, K. Ender, and W. Lechner, *Physical Review Letters* **130**, 220601 (2023).
- [37] M. J. Schuetz, R. S. Andrist, G. Salton, R. Yalovetzky, R. Raymond, Y. Sun, A. Acharya, S. Chakrabarti, M. Pistoia, and H. G. Katzgraber, arXiv preprint arXiv:2412.14976 (2024).
- [38] X. Qiu, P. Zoller, and X. Li, *PRX Quantum* **1**, 020311 (2020).
- [39] J. Park, S. Jeong, M. Kim, K. Kim, A. Byun, L. Vignoli, L.-P. Henry, L. Henriet, and J. Ahn, *Physical Review Research* **6**, 023241 (2024).
- [40] N. Sibalić, J. Pritchard, C. Adams, and K. Weatherill, *Computer Physics Communications* **220**, 319 (2017).
- [41] G. Pelegrí, A. J. Daley, and J. D. Pritchard, *Quantum Science and Technology* **7**, 045020 (2022).
- [42] [Unitdiskmapping.jl](#).
- [43] S. R. White, *Phys. Rev. Lett.* **69**, 2863 (1992).
- [44] S. R. White, *Phys. Rev. B* **48**, 10345 (1993).
- [45] U. Schollwöck, *Annals of Physics* **326**, 96 (2011), january 2011 Special Issue.
- [46] M. Fishman, S. R. White, and E. M. Stoudenmire, *SciPost Phys. Codebases* , 4 (2022).
- [47] M. Fishman, S. R. White, and E. M. Stoudenmire, *SciPost Phys. Codebases* , 4 (2022).